





THz streak camera performance for single-shot characterization of XUV pulses with complex temporal structures

TIM OELZE,¹ OLENA KULYK,² BERND SCHÜTTE,³  ULRIKE FRÜHLING,^{4,5} EVA KLIMEŠOVÁ,² BARTHOLOMÄUS JAGIELSKI,¹ LAURA DITTRICH,¹ MARKUS DRESCHER,^{4,5} RUI PAN,⁶ NIKOLA STOJANOVIC,^{6,7} VITALY POLOVINKIN,² KRISHNA P. KHAKUREL,² KERSTIN MUEHLIG,⁸ IVETTE J. BERMUDEZ MACIAS,⁶ STEFAN DÜSTERER,⁶ BART FAATZ,⁶ JAKOB ANDREASSON,^{2,8} MAREK WIELAND,^{4,5} AND MARIA KRIBUNOVA^{1,2,*} 

¹*Institut für Optik und Atomare Physik, Technische Universität Berlin, Strasse des 17. Juni 135, ER 1-1, 10623 Berlin, Germany*

²*ELI Beamlines, Institute of Physics, Czech Academy of Sciences, Na Slovance 2, 18221 Prague, Czech Republic*

³*Max-Born-Institut, Max-Born-Str. 2A, 12489 Berlin, Germany*

⁴*Institut für Experimentalphysik, Universität Hamburg, Luruper Chaussee 149, 22761 Hamburg, Germany*

⁵*Center for Ultrafast Imaging, Luruper Chaussee 149, 22761 Hamburg, Germany*

⁶*Deutsches Elektronen-Synchrotron DESY, Notkestrasse 85, 22607 Hamburg, Germany*

⁷*DLR – Institute for Optical Sensor Systems, Rutherfordstraße 2, 12489 Berlin, Germany*

⁸*Uppsala University, Department of Cell and Molecular Biology, Husargatan 3, 75237 Uppsala, Sweden*
**maria.krikunova@physik.tu-berlin.de*

Abstract: The THz-field-driven streak camera has proven to be a powerful diagnostic-technique that enables the shot-to-shot characterization of the duration and the arrival time jitter of free electron laser (FEL) pulses. Here we investigate the performance of three computational approaches capable to determine the duration of FEL pulses with complex temporal structures from single-shot measurements of up to three simultaneously recorded spectra. We use numerically simulated FEL pulses in order to validate the accuracy of the pulse length retrieval in average as well as in a single-shot mode. We discuss requirements for the THz field strength in order to achieve reliable results and compare our numerical study with the analysis of experimental data that were obtained at the FEL in Hamburg - FLASH.

© 2020 Optical Society of America under the terms of the [OSA Open Access Publishing Agreement](#)

1. Introduction

Short-wavelength pulses of ultra-short duration and high intensity as delivered by extreme ultraviolet (XUV) and (soft) X-ray free-electron lasers (FELs) have opened new frontiers in atomic and molecular physics, non-linear spectroscopy, solid density plasma physics, photochemistry, and structural biology [1–5]. The accurate knowledge of temporal characteristics of the FEL pulses is essential for a large number of applications. In particular, structural studies aim to shorten the pulse duration in order to outrun radiation damage during the exposure [6–8]. The FEL-pulse duration is related to the rate of energy deposition into the sample. Therefore, it is an essential parameter for understanding the electronic response of atoms [9–11], nanoparticles [12–14], and solids [15]. Moreover, the convolution of the pump and probe temporal pulse profiles defines the time resolution in conventional pump-probe experiments.

In high-gain single-pass FELs the radiation is emitted in short coherent spikes via the self-amplified spontaneous emission (SASE) process. The phase relationship between individual

spikes is random [16–18]. The coherence time is related to the SASE gain bandwidth. In the frequency domain, spikes are also observed in single-shot spectra [17,18]. The width of the spectral spikes is inversely proportional to the temporal length of the photon pulse. The complex spectral and temporal structure of SASE FEL pulses makes their diagnostics challenging.

To provide to a broad user community reliable information on the temporal structure of FEL pulses, a number of direct and indirect diagnostics techniques has been developed [18–20]. Indirect methods are based on the electron bunch duration measurements in the time as well as in the frequency domain [17,21]. Other indirect methods utilize statistical SASE properties and investigate either statistical fluctuations of the radiation energy or spectral intensity correlations in the emitted spectra [16,17]. An additional approach based on advanced machine learning algorithms has been developed recently [22]. Indirect techniques now enable a reliable prediction of the temporal characteristics of the FEL pulses. However, their verification and calibration requires photon pulse measurements in the time domain. Therefore, several cross-correlation schemes with externally synchronized optical laser pulses have been developed [19,20]. These methods are based either on the FEL-induced changes of the optical properties of materials [23–25] or on the laser-dressed photoelectron spectroscopy in atomic gas media, so called generation of side-bands [26,27]. When the X-ray pulse duration approaches the oscillation period of the dressing laser, the side-band generation regime transfers into the streaking regime as it is shown by numerical calculations in Ref. [28]. The light field driven streak camera is actively used in the attosecond pulse metrology [29]. For metrology of femtosecond FEL pulses, a terahertz (THz) field is used for streaking [30].

Following the first demonstration of the THz-field streaking [30] this technique has been successfully implemented for measurements of fs SASE FEL pulses [31] as well as for pulses produced by the high harmonic generation (HHG) [32,33]. The main advantage of the streak camera measurement is its capability to extract the FEL pulse duration and the arrival time jitter of each FEL shot from few simultaneously recorded spectra. A time-consuming THz-XUV delay scan that is essential for the characterization of the THz field needs to be performed only prior to the measurement. The single-shot capability of the streak camera motivated the efforts towards its integration into the beamline photon diagnostics at several user facilities [34–36]. The high interest of the photon science community to streak camera measurements at FEL and other laser facilities triggers a high demand on the efficient data analysis procedures that are able to extract time information from a limited number of measurements [20,37].

In the current study we investigate the performance of a THz streak camera for measurements of SASE FEL pulses with pulse lengths of about 100 fs full-width-at-half-maximum (FWHM). We numerically simulate SASE FEL pulses and validate the accuracy of the XUV pulse length retrieval in average and in single-shot mode. Three approaches that are able to extract pulse length from a limited number of measurements are considered. We discuss the requirements for the THz field strength in order to achieve a reliable pulse length retrieval and use this knowledge to analyse streaking measurements performed at the FEL in Hamburg - FLASH. Our results help to optimize the THz based streak camera performance and contribute to the development of efficient data analysis routines in order to provide machine diagnostics and users of experimental end-stations with a fast and reliable feedback.

2. THz streaking principle

In a THz streak camera experiment the ionizing XUV pulse is collinearly overlapped with the laser streaking field in a gas medium. The period of the laser streaking field has to be longer than the XUV pulse duration. Therefore, THz field is used for diagnostics of femtosecond XUV pulses [30–33,36,38] and near infra-red (NIR) field is used for diagnostics of attosecond pulses [29,39–42]. The presence of the laser field introduces an additional momentum to the electrons that are released into the continuum state during the interaction of the XUV pulse with the atoms.

By changing the relative time delay τ between the XUV pulse and the laser streaking field a series of electron kinetic energy spectra $I(W, \tau)$, so called streaking spectrogram, is measured, with W being the kinetic energy of the electron in the final continuum state. The single active electron approximation in combination with the strong field approximation is used to describe the electron spectrum [39,40]:

$$I(W, \tau) = \left| \int_{-\infty}^{\infty} dt e^{i\phi(t)} \mathbf{d}_{p(t)} \mathbf{E}_{XUV}(t - \tau) e^{i(W+I_p)t} \right|^2. \quad (1)$$

Here $\mathbf{d}_{p(t)}$ is the dipole transition matrix element from the ground to the continuum state. Far from any resonances $\mathbf{d}_{p(t)}$ is typically considered to be a constant. $\mathbf{p}(t) = \mathbf{p}_0 + \mathbf{A}(t)$ is the instantaneous momentum of the free electron in the laser streaking field $\mathbf{E}_{streak}(t)$ with \mathbf{p}_0 being the initial electron momentum without streaking field and $\mathbf{A}(t)$ being the vector potential that is given by $\mathbf{E}_{streak}(t) = -\partial\mathbf{A}/\partial t$. $\mathbf{E}_{XUV}(t)$ is the electric field of the XUV pulse, I_p is the ionization potential of the atom and $\phi(t)$ is the phase accumulated in the continuum state. We note the use of the atomic units throughout the manuscript ($e = m_e = \hbar = 1$) unless further specified. Equation (1) shows that the laser dressing field introduces a temporal phase modulation on the electron wave packet and therefore the light-field-driven streak camera is often considered as *an ultrafast electron phase modulator* [40,41].

Following considerations are discussed in Ref. [40,41], namely, (i) a linearly polarized streaking field $E_{streak}(t) = E_0(t) \cos(\omega_{streak}t)$ has an envelope that is long enough to apply slowly-varying envelope approximation, (ii) electrons are emitted in the direction of the laser polarization, and (iii) it is assumed that $U_p(t) = E_0^2(t)/4\omega_{streak}^2 \ll W$, where $U_p(t)$ is the ponderomotive potential of the electron in the laser field and ω_{streak} is the angular frequency of the streaking field. In this case it can be shown that close to the zero-crossing point of the vector potential $A(t)$, the phase term in the Eq. (1) can be approximated to

$$\phi(t) \approx \sqrt{\frac{8WU_p}{\omega_{streak}^2}} \left(1 - \frac{\omega_{streak}^2 t^2}{2}\right). \quad (2)$$

Introducing the streaking speed $\alpha = \sqrt{8U_p W} \omega_{streak}$ into Eq. (2)

$$\phi(t) \approx -\frac{\alpha t^2}{2} \quad (3)$$

reveals that the phase modulation $\phi(t)$ is quadratic in time and, thus, the electron wavepacket experiences a linear streaking in energy $dW/dt = -\partial^2\phi(t)/\partial t^2 = \alpha$ [40,41]. This allows to apply several simplified procedures to extract information on the pulse duration from the streaking measurements as discussed in the following section.

3. Procedures to extract pulse durations from the THz streaking measurements

To extract the duration of FEL pulses from measured photoelectron spectra $I(W, \tau)$, we consider three approaches that require only a limited number of measured spectra: (i) Gaussian approximation - it is based on the analytical solution of the integral in Eq. (1) by approximating the electric field of the XUV pulse $E_{XUV}(t)$ with a Gaussian amplitude envelope and a quadratic phase [30,37]; (ii) Linear streaking - it is valid at sufficiently high streaking speed α , i.e. in the so-called linear streaking regime. The temporal phase of the XUV pulse is neglected by this approach and the temporal profile of the FEL pulse is retrieved by a direct projection of $I(W, \tau)$ onto the time axis [20,31,42]; (iii) Simplified chronocyclic tomography (CT) - this approach treats the streaking effect as a shear of the Wigner distribution on the time-axis [40,43,44] according to Eq. (3). Simplified CT holds the potential to retrieve the temporal structure of the XUV pulse including its temporal phase [40,43,44].

3.1. Gaussian approximation

Consider the electric field $E_{XUV}(t)$ of the XUV pulse to have a Gaussian amplitude envelope and a quadratic phase:

$$E_{XUV}(t) = \exp(-at^2) \exp\left(i\left(\omega_0 t + \frac{bt^2}{2}\right)\right), \quad (4)$$

where the parameter a is related to the root mean square (rms) pulse length τ_{XUV} of the XUV intensity $I_{XUV}(t) = |E_{XUV}(t)|^2$ according to $\tau_{XUV} = 1/(2\sqrt{a})$. Here and further in the text we refer to the rms length of the intensity profile of the pulse as τ_{XUV} , which is related to the FWHM of the intensity profile as $T_{XUV} = 2\sqrt{2\ln 2}\tau_{XUV} \simeq 2.35\tau_{XUV}$. In Eq. (4) ω_0 is the carrier frequency and b is the linear chirp parameter that describes the linear sweep of the instantaneous frequency $\omega_{inst}(t) = \omega_0 - bt$. Substitution of Eq. (3) and Eq. (4) into Eq. (1) provides an analytical solution for the integral and allows direct calculation of τ_{XUV} and b from streaked spectra [30,37].

$$\tau_{XUV} = \sqrt{\frac{(\sigma_+^2 + \sigma_-^2) - 2\sigma_0^2}{2\alpha^2}}, b = \frac{\sigma_+^2 - \sigma_-^2}{4\alpha\tau_{XUV}^2}, \quad (5)$$

where σ_0 , σ_+ and σ_- represent the rms spectral bandwidths of unstreaked spectra and, respectively, streaked spectra with positive $\alpha > 0$ and negative $\alpha < 0$ streaking speed. Spectra with the spectral bandwidths σ_+ and σ_- are measured at the zero-crossing points of the vector potential $A(t)$ using electron spectrometers installed parallel and antiparallel with respect to the electrical field vector of the streaking field [30,37]. Spectrum with the spectral bandwidth σ_0 is measured in the absence of the streaking field. It is determined from the online measurement of the XUV pulse spectrum as described in section 5.1. The streaking speed α is determined from the analysis of streaking spectrograms as described in section 5.2.

The Gaussian approximation has been implemented for the retrieval of SASE FEL pulses at FLASH [30,37], HHG pulses [32,33] as well as seeded FEL pulses [38] with several tens of femtoseconds pulse duration. All studies report good agreement between retrieved and expected photon pulse durations. Retrievals of the chirp of HHG pulses indicate a reproduction of the decrease of the chirp parameter with increasing harmonic order [33]. Analyses of SASE FEL [30,37] and seeded FEL [38] photon pulses reveal a linear chirp that is attributed to the linear energy chirp in the electron bunch.

3.2. Linear streaking regime

When the streaking speed is large ($|\alpha| \gg |b|$), i.e. in the so-called linear streaking regime [20,31,42], the τ_{XUV} can be retrieved from the direct projection of the rms streaked spectral bandwidth σ_{streak} onto the time axis according to $\tau_{XUV} = \sigma_{streak}/|\alpha|$. This relationship can also be deduced from Eq. (5) when $\sigma_+ \simeq \sigma_- \gg \sigma_0$ is considered. Therefore, at large streaking speeds both approaches should be applicable for pulses with arbitrary shapes. In our study we tested whether the use of an average streaked bandwidth $(\sigma_+ + \sigma_-)/2\alpha$ would provide a more accurate estimation of the XUV pulse length:

$$\tau_{XUV} = \frac{\sigma_+ + \sigma_-}{2|\alpha|}. \quad (6)$$

The linear streaking approach has successfully been implemented to retrieve SASE FEL pulses at FLASH [31] and LCLS [42] with few fs pulse durations.

3.3. Simplified chronocyclic tomography

Another approach to retrieve a pulse in the time domain from measurements in the frequency domain is to use tomographic techniques [40,43,44]. In this approach the spectral $I(\omega)$ and the

temporal $I(t)$ intensity profiles of a pulse are considered as frequency and time marginals of the Wigner distribution function $W_{Wigner}(t, \omega)$, i.e. its projections onto the frequency (recall that the photon energy of a pulse is $\hbar\omega$) and the time axis, respectively:

$$I(\omega) = \int dt W_{Wigner}(t, \omega), I(t) = \int \frac{d\omega}{2\pi} W_{Wigner}(t, \omega). \quad (7)$$

In chronocyclic tomography (CT) a large number of projections of the rotated Wigner distribution is measured and then a back-projection algorithm is applied to retrieve the Wigner distribution from a set of measured projections.

In simplified CT an electric field of a pulse can be retrieved using one projection of the Wigner function and its angular derivative [40,43,44]. According to Eq. (2) streaking with a streaking speed α at the zero-crossing points of the vector potential $A(t)$ is considered as a quadratic temporal phase modulation that corresponds to a shear of the Wigner function along the frequency axis in the chronocyclic (t, ω) space: $W_{WignerOUT}(t, \omega) = W_{WignerIN}(t, \omega + \alpha t)$. Following the discussion in Refs. [40,43,44] it can be shown that for streaking speed α close to zero:

$$\left. \frac{\partial I_\alpha}{\partial \alpha} \right|_{\alpha=0} = - \frac{\partial}{\partial \omega} \left[I(\omega) \frac{\partial \varphi}{\partial \omega} \right]. \quad (8)$$

This means that the group delay $\partial \varphi / \partial \omega$ of a pulse can be obtained from the frequency marginal of the Wigner function $I(\omega)$ and its angular derivative $\partial I_\alpha / \partial \alpha$. The angular derivative $\partial I_\alpha / \partial \alpha$ is estimated via two spectra I_+ and I_- measured at two opposite streaking speeds: $(I_+ - I_-) / 2$. The simplified CT has been verified experimentally in the optical regime [43] and is proposed theoretically for the evaluation of light-field streaking spectrograms [40]. In the current study we investigate the applicability of this approach to SASE FEL pulses with complex temporal and spectral structures.

4. Numerical study of THz streak camera performance

In the following section we describe how model pulses with similar pulse shapes as expected in the experiment are generated numerically. Further, Eq. (1) is used to calculate streaked spectra at zero-crossing points of the vector potential at different streaking speeds α . The frequency of the THz field is kept at 1 THz while the field strength is varied in a range that is typical for the THz streaking experiment (with one exception of very low streaking speed $\alpha=0.2$ meV/fs) as summarized in Table 1. Then we apply the Gaussian approximation, the linear streaking as well as the simplified CT to extract the rms pulse duration from numerically simulated streaking spectra. In order to evaluate numerically the performance of all three different pulse retrieval approaches we compare the retrieved with the original rms pulse duration.

Table 1. THz field strengths and resulting parameters as used in the simulation: streaking speed α , amplitude of streaking field E_0 , ponderomotive potential U_p , maximal kinetic energy shift ΔW_{max} experienced by the electron with initial kinetic energy of $W_0=71$ eV in the streaking field, relative spectral broadening (averaged over all shots) $\Delta\sigma/\sigma_0$ due to streaking, defined as a ratio between de-convoluted streaked bandwidth $\Delta\sigma = \sqrt{\sigma_{streak}^2 - \sigma_0^2}$ and unstreaked bandwidth σ_0 .

E_0 (MV/m)	0.05	0.2	0.5	1.2	5.8	12	23
α (meV/fs)	0.2	1	2	5	25	50	100
U_p (meV)	0.002	0.06	0.2	1.6	37	160	580
ΔW_{max} (eV)	0.04	0.2	0.4	1	4.7	10	20
$\Delta\sigma/\sigma_0$	0.05	0.2	0.5	1.3	6.3	12.7	23.1

4.1. Generation of model pulses

The SASE process starts from the shot noise in the electron bunch. This results in characteristic spectral and temporal intensity profiles of the photon pulses consisting of multiple random spikes with random phase fluctuations between individual spikes [18,45]. To mimic the random structure of the SASE FEL pulses numerically, the electric field and phase are constructed in the spectral domain by using a pseudo-random Wiener processes. To set an appropriate limit to the bandwidth of the numerical XUV pulses the envelope of the field is multiplied with a Gaussian profile. The temporal profile and the temporal phase of a pulse are calculated via the Fourier transform. The width of the Gaussian function as well as a drift parameter in the random walk process are chosen randomly. The main criteria in the choice of parameters is to match the temporal and spectral bandwidth as well as the coherence time of numerically generated pulses with FEL pulse properties expected in the experiment. Finally, about 3000 pulses with an average FWHM spectral bandwidth of (1.1 ± 0.2) eV (standard deviation), FWHM pulse duration of (103 ± 33) fs (standard deviation) and a coherence time of (10.6 ± 1.3) fs (standard deviation) are selected for modelling of the streaking process. Our approach is similar to the one used in Ref. [46] to model FEL pulses produced in the SASE operation mode.

A representative example of a numerically generated pulse is shown in Fig. 1. The upper photon energy scale in Fig. 1(a) shows the spectral intensity profile of the XUV pulse of 92.5 eV central photon energy. Ionization of atomic gas results in the electron distribution that (under low irradiation intensity, low atomic gas density conditions and far from any resonances) is considered as a replica of the XUV pulse. The lower electron kinetic energy scale in Fig. 1(a) corresponds to the electron kinetic energy spectrum resulting from the release of Ne(2p) electrons from a Ne gas target after absorption of XUV photons. Note, that the average spectral bandwidth of FEL pulses is 1.1 eV (FWHM) in our simulation and 1.25 eV (FWHM) in the experiment, i.e. substantially larger than the spin-orbit splitting of Ne $2p_{1/2}$ and $2p_{3/2}$ states with the corresponding ionization potentials of 21.7 eV and 21.6 eV. Therefore, the center of the electron kinetic energy spectrum in Fig. 1(a) is shifted by 21.65 eV (the average ionization potential I_p of Ne(2p) electrons) with respect to the central XUV photon energy. The temporal intensity profile shown in Fig. 1(b) is composed of multiple spikes in accordance with the expected FEL pulse structure [18,45].

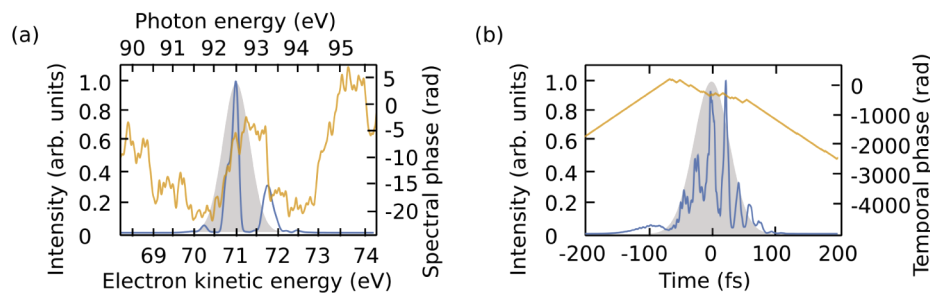


Fig. 1. (a) Spectral intensity profile (blue solid line) and spectral phase (orange solid line) and (b) temporal intensity profile (blue solid line) and temporal phase (orange solid line) of the numerically generated model pulse. The Gaussian profile with the equivalent rms spectral and temporal width as calculated according to Eqs. (9) and (10) is shown for comparison (grey shaded area).

To calculate spectral σ_{XUV} and temporal τ_{XUV} bandwidth from simulated spectral $I(W)$ and temporal $I(t)$ intensity profiles the corresponding equations for weighted sample standard

deviation are used:

$$\sigma_{XUV} = \sqrt{\frac{\sum_{i=1}^N I(W_i) (W_i - \mu_{\sigma}^*)^2}{\sum_{i=1}^N I(W_i)}} \quad \text{with} \quad \mu_{\sigma}^* = \frac{\sum_{i=1}^N W_i I(W_i)}{\sum_{i=1}^N I(W_i)}, \quad (9)$$

and

$$\tau_{XUV} = \sqrt{\frac{\sum_{i=1}^N I(t_i) (t_i - \mu_{\tau}^*)^2}{\sum_{i=1}^N I(t_i)}} \quad \text{with} \quad \mu_{\tau}^* = \frac{\sum_{i=1}^N t_i I(t_i)}{\sum_{i=1}^N I(t_i)}. \quad (10)$$

τ_{XUV} is calculated in the range of ± 400 fs and σ_{XUV} from 60 eV to 90 eV. To implement the Gaussian approximation, we assume that the spectral and temporal profile is approximated by the Gaussian shape with the corresponding equivalent rms spectral and temporal widths as shown in Figs. 1(a) and 1(b) by the grey shaded area.

4.2. Results of pulse reconstruction for numerically generated pulses

Figure 2 summarizes results of pulse retrievals using the Gaussian approach, linear streaking as well as the simplified CT as a function of streaking speed. Statistical variations and absolute accuracies for retrieval of individual pulses are shown in Fig. 3. At each streaking speed (see Table 1) the analyses are performed on the same set of 3000 numerically generated pulses. We compare $\langle \tau_{retr}/\tau_{orig} \rangle$ - the average of ratios between the retrieved τ_{retr} and the original τ_{orig} rms pulse lengths. To characterize statistical variations between retrieved τ_{retr} and original τ_{orig} rms pulse lengths, we calculate the Pearson correlation coefficient $r_{\tau_{orig}, \tau_{retr}}$ between the two variables τ_{orig} and τ_{retr} at different streaking speeds. The Pearson correlation coefficient $r_{\tau_{orig}, \tau_{retr}} = \text{COV}(\tau_{orig}, \tau_{retr}) / (\sigma_{\tau_{orig}} \sigma_{\tau_{retr}})$ is defined as a ratio between covariance and corresponding standard deviations $\sigma_{\tau_{orig}}$ and $\sigma_{\tau_{retr}}$.

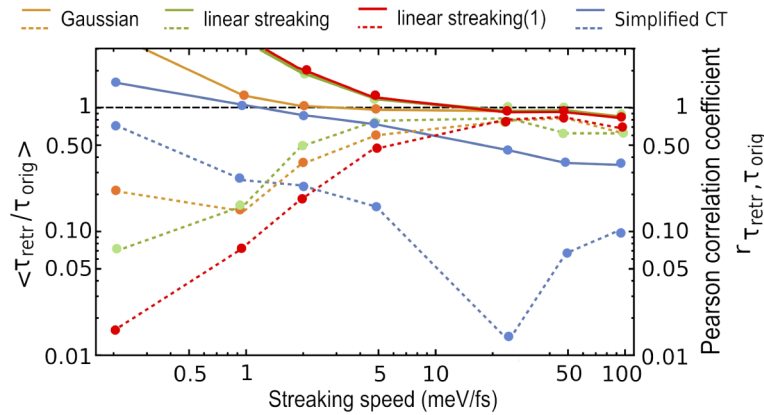


Fig. 2. Average of ratios between reconstructed and original rms pulse lengths (solid lines, left scale) as well as their correlations (dashed lines, right scale) studied at different streaking speeds. Orange - results of pulse reconstruction using Gaussian approach, green and red - using linear streaking and blue - using simplified chronocyclic tomography (CT). For linear streaking (green) we use Eq. (6) while for linear streaking (1) (red) we use the relationship $\tau_{XUV} = \sigma_{streak}/|\alpha|$ to estimate τ_{retr} .

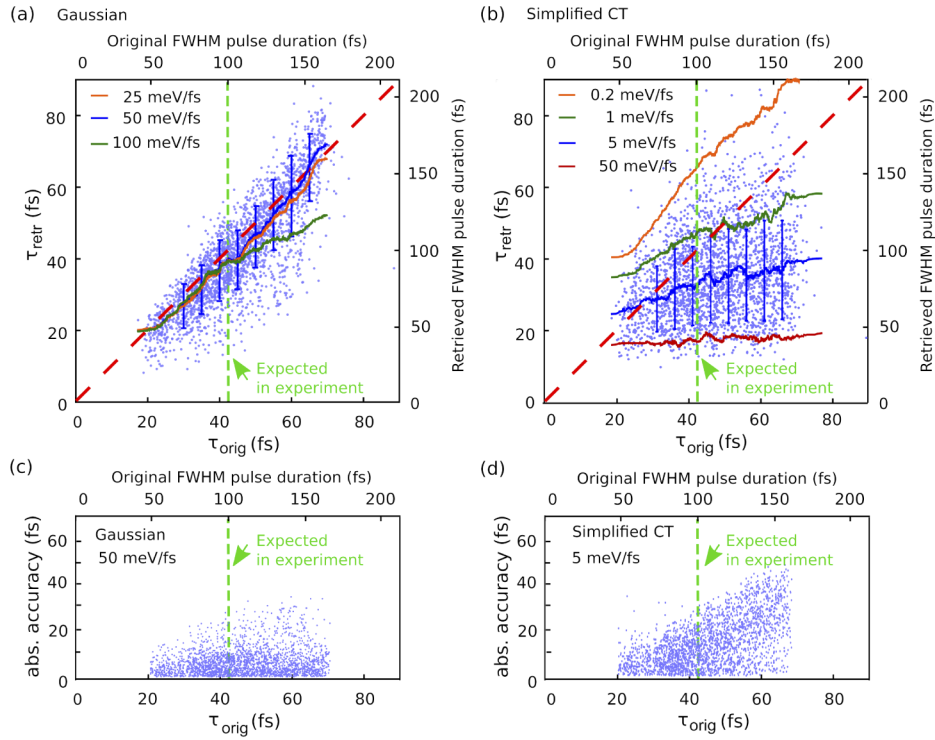


Fig. 3. Statistical variation between original τ_{orig} and retrieved τ_{retr} rms pulse lengths retrieved by (a) Gaussian approach and (b) simplified chronocyclic tomography (CT). The blue points show shot-to-shot retrieval at streaking speed $\alpha=50$ meV/fs in (a) and at $\alpha=5$ meV/fs in (b). The solid lines show the running median over 100 data-points and the bars the related standard deviations. The corresponding streaking speeds are indicated in the legend. The dashed red line corresponds to $\tau_{orig}/\tau_{retr} = 1$. Absolute accuracy of the rms pulse length retrieval for Gaussian approach at 50 meV/fs (c) and for simplified CT at 5 meV/fs streaking speed (d).

As it follows from the comparison of τ_{orig} and τ_{retr} the linear approach should not be used at very small streaking speeds. According to the Table 1 at streaking speeds $\alpha \leq 5$ meV/fs the streaked spectral widths are comparable to the non-streaked width. This results in overestimation of the pulse lengths which is manifested by large $\langle \tau_{retr}/\tau_{orig} \rangle$ as observed in the Fig. 2.

Reconstruction by Gaussian and linear streaking approaches provides very similar results (Fig. 2, orange, green and red solid and dashed lines). With increasing streaking speed the average of ratios $\langle \tau_{retr}/\tau_{orig} \rangle$ and the correlation coefficient $r_{\tau_{orig}, \tau_{retr}}$ are approaching 1. At $\alpha \geq 25$ meV/fs the difference between the two methods almost disappears. For linear streaking we have used the relationship $\tau_{XUV} = \sigma_{streak}/|\alpha|$ (red solid and dashed lines) as well as Eq. (6) with an average streaked bandwidth (green solid and dashed lines) in order to estimate the XUV pulse lengths. The average of ratios $\langle \tau_{retr}/\tau_{orig} \rangle$ is nearly the same for both methods at all streaking speeds (green and red solid lines are overlapping). At lower streaking speeds $\alpha < 25$ meV/fs the correlation coefficient $r_{\tau_{orig}, \tau_{retr}}$ is higher when Eq. (6) is used, while at higher streaking speeds $\alpha \geq 25$ meV/fs both approaches show no difference. Our analysis indicates that at large streaking speeds as typically used in THz streaking experiments [30–33] both Gaussian and linear approximations provide reasonable estimation of the mean pulse duration. For Gaussian approach implemented at $\alpha = 50$ meV/fs streaking speed the absolute accuracy is around 10 fs

for most of reconstructed pulses (Fig. 3(c)) and is found to be very similar for the linear streaking approach (data not shown).

In contrast to the Gaussian and the linear streaking approach, for simplified CT the average of ratios $\langle \tau_{retr}/\tau_{orig} \rangle$ is close to 1 only at very low streaking speed values $\alpha < 5$ meV/fs (Fig. 2, blue solid line). The Pearson correlation coefficient is very low (Fig. 2, blue dashed line) indicating a very large spread between τ_{retr} and τ_{orig} . This is analysed in Fig. 3 that compares shot-to-shot XUV pulse retrieval by the Gaussian (a) vs. the simplified CT (b) approach. For the Gaussian approach (Fig. 3(a)) the standard deviation of data points from a median value (spread of data points) is about 15 fs and is found to be similar for all streaking speeds. Running median values (solid lines in Fig. 3(a)) are close to the $\tau_{orig}/\tau_{retr} = 1$ line (red dashed line). The deviation for longer ($\tau_{orig} > 50$ fs) pulses at large streaking speed $\alpha = 100$ meV/fs (green solid line) is explained by the numerical artefacts in the simulation, namely, a broadening of streaked spectra becomes very large (Table 1) and approaches the whole length of the electron energy axis used in the simulation.

For the simplified CT (Fig. 3(b)) the spread between the original τ_{orig} and the retrieved τ_{retr} pulse lengths is substantially larger. The running median line is parallel to the $\tau_{orig}/\tau_{retr} = 1$ line (red dashed line) only at very low streaking speed $\alpha = 0.2$ meV/fs (orange solid line) that is in correspondence with relatively high correlation value of 0.8 at this streaking speed (Fig. 2). However, the retrieved pulse lengths are significantly overestimated (the orange solid line is located above the red dashed line in Fig. 3(b)). With increasing streaking speed τ_{retr} becomes smaller than the original pulse length τ_{orig} . Moreover, τ_{retr} becomes less dependent on τ_{orig} as indicated by the vanishing slope of the running median lines (green, blue and red solid lines). At a streaking speed $\alpha = 50$ meV/fs the retrieved pulse length τ_{retr} becomes independent of τ_{orig} . Figure 3(d) shows that the absolute accuracy at 5 meV/fs streaking speed becomes larger with increasing τ_{orig} . This indicates that the simplified CT might be more sensitive to the lower order phase terms and is getting less applicable for pulses with increasing complexity of the spectral phase. In our simulation the spectral bandwidth was limited to FWHM of (1.1 ± 0.2) eV (standard deviation). Due to this limitation the larger pulse duration corresponds to the increasing complexity of the spectral phase. From Fig. 2 and Fig. 3(b), (d) we conclude that the implementation of simplified CT to pulses with very complex temporal and spectral phase is not straightforward. In accordance with simplifications made in Eq. (8) a possible application of simplified CT is limited to very small streaking speeds, in our case to $\alpha < 5$ meV/fs.

To summarize the results of our numerical study, we have found that for pulses with complex temporal and spectral structure a linear streaking or Gaussian approach needs to be implemented at large streaking speed to provide a reasonable estimation of the pulse duration. The simplified CT algorithm does not provide satisfactory results even at very small streaking speeds. In the following section we discuss the implementation of the Gaussian, the linear streaking and the simplified CT approaches for the analysis of experimental data.

5. THz streaking experiment at FLASH FEL

5.1. Experimental setup

The THz streaking experiment is performed in the unfocused branch of the beamline BL3 [47] and the THz beamline [48] of the FLASH FEL. The FEL is tuned to maximum pulse energy with an electron bunch charge of 0.3 nC and an electron energy of 680 MeV. At these parameters of FEL operation an XUV pulse duration of around ~ 100 fs (FWHM) is expected. Both XUV and THz pulses are generated from the same electron bunch enabling a high level of synchronization of the multi-cycle THz pulse with the XUV pulse [30,48]. In the current study the jitter between XUV and THz pulses was in the order of 10 fs rms as revealed from an analysis of streaking spectrograms. The experimental geometry is shown in Fig. 4(a). In the interaction region XUV pulses of 13.4 nm central wavelength (92.5 eV photon energy) and THz pulses of 3 THz central

frequency (100 μm wavelength) are collinearly overlapped and focused into an atomic gas jet. For balancing the XUV and THz beamline lengths the XUV pulses are delayed and back focused by a spherical Mo/Si multilayer mirror with a focal length of 2.0 m to a spot size of about 100 μm FWHM. The maximum reflectivity of the Mo/Si mirror is at ~ 92.5 eV with a bandwidth of ~ 5 eV FWHM. The THz pulses are focused with an off-axis parabolic mirror of 200 mm focal length to a spot size of ~ 0.5 mm. A band-pass filter (QMC Instruments) was used to reduce the THz spectral bandwidth.

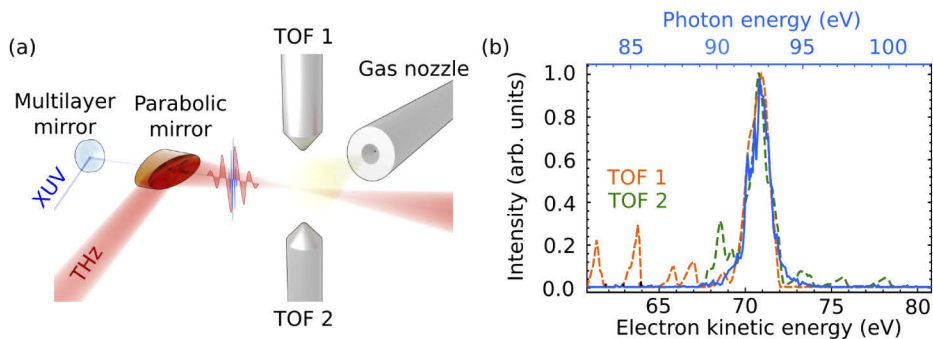


Fig. 4. (a) Experimental geometry. (b) Photon energy spectrum of an XUV pulse (blue solid line, upper scale) and THz field free electron kinetic energy spectra resulting from ionization of Ne(2p) electrons by the same XUV pulse (orange and green dashed lines, lower scale). Electron kinetic energy spectra are measured with two opposite time-of-flight spectrometers - TOF 1 and TOF 2. All spectra are normalized to the area under the main peak.

In order to characterize the THz field as well as to identify zero-crossing points of the THz vector potential for subsequent XUV pulse diagnostic THz streaking spectrograms are obtained by moving the delay line available in the THz-branch [48] with 33 fs steps. Electron kinetic energy spectra resulting from the ionization of Ne atoms by XUV pulses are measured in a single-shot with two opposite time-of-flight (TOF) spectrometers that are installed parallel to the THz polarization direction. This allows to obtain two streaking spectrograms with the same streaking speed value but opposite signs within one XUV-THz time-delay scan (Figs. 5(a) and 5(b)). At each fixed XUV-THz delay stage position relative large data set of 100 to 120 consecutive measurements is obtained. The combination of a time-delay scan for the THz field characterization with the acquisition of single-shot data at each fixed delay line position for further analysis of the XUV pulse durations has been chosen in order to use the limited beamtime more efficiently by postponing the data analysis after the end of the user beamtime. The fluctuating number of single-shots at each time delay is explained by the data acquisition routine. Care was taken to minimize a broadening of the electron spectra by space charge effects as well as to prevent complete ionization of the neutral target within the XUV pulse [12]. Therefore, the XUV beam was strongly attenuated with zirconium foil filters.

Synchronously to the acquisition of the electron kinetic energy spectra the spectrum of the XUV pulse is measured by a variable line spacing grating spectrometer (VLS) (Fig. 5(c)). The VLS is installed upstream and uses a fraction of the same beam that is delivered to the experiment [49]. The VLS spectrum is taken as unstreaked spectrum for the pulse retrieval algorithms. Figure 4(b) shows a representative example of the photon energy spectrum of an XUV pulse (blue solid line, upper scale) measured with the VLS spectrometer and for the same pulse the electron kinetic energy spectra measured with opposite TOF spectrometers in the absence of the THz field (orange and green dashed line, bottom scale). The electron kinetic energy scale is shifted with respect to the photon energy scale by 21.65 eV, i.e. by an average I_p of Ne 2p_{1/2} and 2p_{3/2} states (similar to Fig. 1(a)). All spectra are normalized to the area under the main peak.

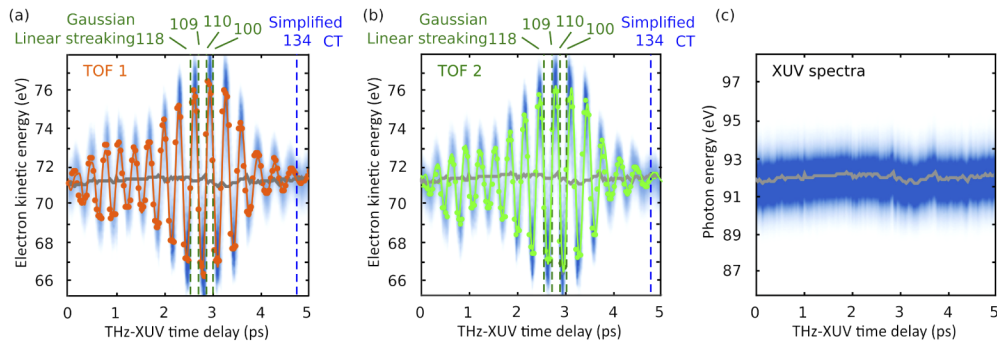


Fig. 5. (a) and (b) streaking spectrograms (color plot) measured with two opposite time-of-flight (TOF) spectrometers. Points are center-of-mass electron energies of Ne(2p) electrons as extracted from the analysis of two streaking spectrograms. Solid lines are fit to the data points with an amplitude modulated sinusoidal function. The zero-crossing points at which pulse retrieval analyses have been performed are indicated by dashed lines - green for Gaussian and linear streaking, blue for simplified chronocyclic tomography (CT). The number of analysed single-shot measurements at each zero-crossing point is indicated on the top. (c) Photon energy spectra of the XUV pulse measured simultaneously to TOF spectra. Spectra are averaged at each time delay step. Grey solid line in each panel indicates the center of mass of averaged XUV spectra.

Peaks appearing in the electron kinetic energy spectra to the left and to the right of the Ne(2p) photoline are artefacts caused mainly by microchannel plate (MCP) dark counts. Both spectra are overlapping well, showing that the spectral bandwidth of the XUV pulse is not cut by the beam propagation through the beamline and, in particular, by the multilayer focusing mirror.

For the careful implementation of the pulse retrieval algorithms an accurate characterization of the THz vector potential is essential. Therefore, at each THz-XUV time-delay an average center-of-mass value in the electron kinetic energy spectra is determined (Figs. 5(a) and 5(b), points) and then fitted by an amplitude modulated sinusoidal function (Figs. 5(a) and 5(b), solid line). This allows one to obtain the exact positions of the zero-crossing points as well as the streaking speed values. Following THz field parameters have been extracted: maximal electrical field strength 19 MV/m, maximal vector potential $A=4 \times 10^{-5}$ V s/m, maximal streaking speed $\alpha=95$ meV/fs, THz frequency 3.14 THz and a linear chirp of 0.136 THz/ps.

5.2. FEL pulse retrieval

The pulse retrieval algorithms are implemented by taking single-shot spectra measured with two opposite spectrometers at zero-crossing points of the vector potential (streaked spectra) and one XUV photon energy spectrum measured with the VLS spectrometer (unstreaked spectrum). At FLASH the THz pulse is multi-cycle as shown in Figs. 5(a) and 5(b). This allows to select the optimal streaking speed for the pulse retrieval in accordance with our numerical study. For the Gaussian and the linear streaking approach zero-crossing points that are located close to the pulse maximum amplitude with streaking speed $\alpha > 85$ meV/fs (green dashed lines in Figs. 5(a) and 5(b)) have been selected. Correspondingly for the implementation of simplified CT it is essential to keep the streaking speed as low as possible. Therefore, a region on the edge of the THz pulse with the streaking speed of 5 meV/fs has been selected (blue dashed line in Figs. 5(a) and 5(b)). The number of analysed single-shot measurements at each zero-crossing point is indicated in Figs. 5(a) and 5(b) on the top. For the Gaussian and the linear streaking approaches the time delay steps closest to the green dashed lines in Figs. 5(a) and 5(b) are selected. The fluctuating numbers of measurements at the corresponding time delay step are due to the data acquisition

routine. Equation (9) applied in the range of 60 eV to 90 eV is used to calculate the rms spectral bandwidths. Note that the presence of noise spikes might lead to a possible overestimation of the rms spectral bandwidth and, thus, according to Eqs. (5) and (6), to the overestimation of the pulse duration. The choice of the broader spectral range and of the weighted standard deviation given by Eq. (9) for the calculation of the rms width helps to suppress the contribution of noise spikes. For the simplified CT it is essential to perform the measurement exactly at the zero-crossing point in order to eliminate the shift of the electron kinetic energy spectra due to the streaking. We have analysed the difference between the center-of-mass of the Ne(2p) photoline in streaked with respect to unstreaked spectrum at three time delay steps that are located close to the blue dashed line in Figs. 5(a) and 5(b). In case this difference is below 150 meV the corresponding measurement is selected for further analysis. In total 134 shots are selected. Figure 6 shows representative examples of single-shot spectra taken for analysis with the simplified CT (a, c) and the Gaussian as well as the linear streaking approaches (b, d).

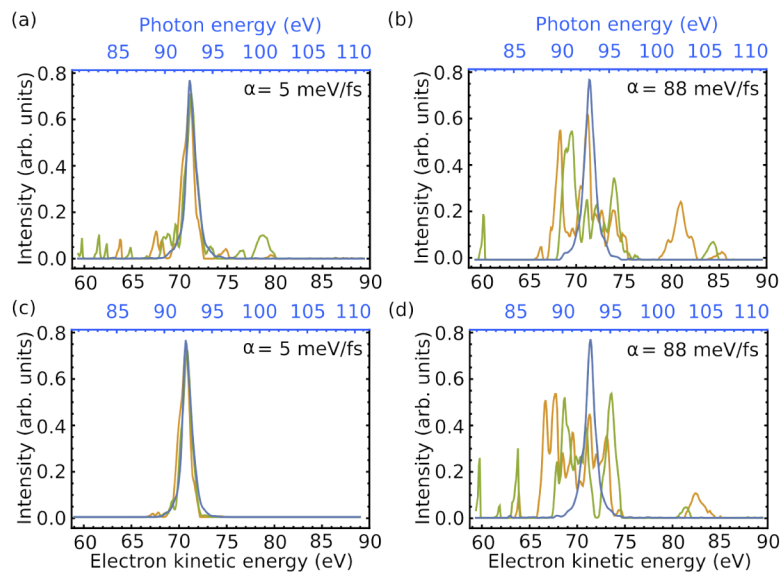


Fig. 6. Single-shot unstreaked (blue) and two corresponding streaked spectra (green and orange) that are further analysed by the simplified chronocyclic tomography (a) and Gaussian as well as linear streaking approaches (b) and (d). (c) the same spectra as shown in (a) after applying a Gaussian filter to suppress the noise signal on the edges of the Ne(2p) photoline. All spectra are normalized to the area under the main peak. The streaking speed α is shown in the legend.

Figure 7(a) shows the results of the single-shot analysis using the Gaussian (orange bars) and the linear streaking (blue bars) approaches. In case of the linear streaking Eq. (6) is applied. Both histograms are very similar (grey bars represent an overlap between histograms related to Gaussian and linear streaking). This is in correspondence with our numerical study that reveals almost no difference between the two methods at large streaking speeds. For the Gaussian approach the average maximum of the histogram weighted with the number of samples in each bin is at 97 fs and the rms width of the distribution is 17 fs. For the linear streaking approach the weighted average maximum of the histogram is at 100 fs and the rms width of the distribution is 16 fs. The analysis performed on spectra that are averaged over all shots in the histogram reveals a slightly larger (with respect to the weighted average maximum of the histogram) pulse duration of 105 fs (FWHM) for the Gaussian and of 110 fs (FWHM) for the linear streaking approach. This can be explained by the shot-to-shot energy jitter of FEL pulses (visible in the

center-of-mass fluctuations of photon energy spectra in Fig. 5(c)). As observed, averaging of spectra would cause a spectral broadening leading to the overestimation of the pulse duration.

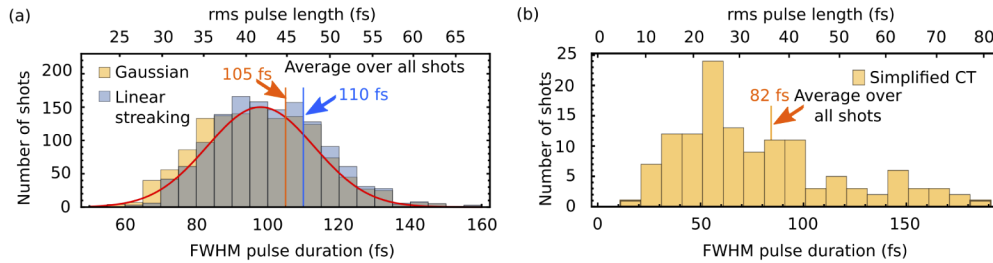


Fig. 7. Results of FEL pulse retrieval using (a) Gaussian as well as linear streaking (colour-coded orange and blue) and (b) simplified chronocyclic tomography (CT) plotted as a histogram. FWHM pulse durations resulting from analysis of spectra that were initially averaged over all shots are indicated by the vertical lines. The red solid curve in (a) shows Gaussian pulse retrieval implemented on numerically generated pulses with FWHM of 100 fs and with 2.5 fs rms width of the distribution.

The results of our pulse retrieval are in good correspondence with the 100 fs FWHM photon pulse duration that is expected from the parameters of the machine operation. The rms width of the retrieved distribution may either originate from natural shot-to-shot fluctuations of the FEL pulse durations or from the uncertainty of the method. The latter is mainly caused by the limitations in the description of pulses with complex temporal and spectral structures by their rms widths. In particular, the rms pulse width is known to overestimate small contributions to the signal at the edges of a pulse (not to be confused with the noise spikes). Note that expected absolute accuracy of linear and Gaussian approaches as estimated from our numerical simulations is around 10 fs (Fig. 3(c)). Additionally, in order to estimate the uncertainty related to the method we perform a numerical test. From the distribution of 3000 numerically generated pulses (Section 4) the pulses with an average pulse duration of 100 fs (FWHM) and a very narrow width of the distribution of 2.5 fs rms are preselected. We then apply the Gaussian approach to this selected distribution. The corresponding analysis results in the same 100 fs (FWHM) pulse duration. However, the width of the distribution is 15 fs rms. This is substantially broader than the initial 2.5 fs rms width but comparable with the width of the distribution obtained from the experimental data (red solid line in Fig. 7). Therefore we suggest that the spread of reconstructed pulse lengths is mainly related to the accuracy of the method rather than to fluctuations of FEL pulse lengths in our experimental run or to other possible sources of noise.

To implement the simplified CT approach a small streaking speed and the possibility to determine the exact streaking speed value are essential. In the streaking spectrogram shown in Fig. 5 we were able to implement the simplified CT approach only at one zero-crossing point (blue dashed line). Results of single-shot analyses are shown in the histogram in Fig. 7(b). The distribution of the retrieved pulse lengths is comparably broad. For the CT approach the information on the spectral phase is encoded in small changes of the spectral amplitude. Therefore, care is taken to select spectra with almost no shift between the center-of-mass in the VLS spectrum (Fig. 6(a), blue line) and the center-of-mass of Ne(2p) photoline in streaked spectra (Fig. 6(a), green and orange lines). Moreover, the method is very sensitive to the noise present in the single-shot electron spectra (note the spikes in green and orange spectra in Fig. 6(a)). A Gaussian filter is used to suppress these contributions (Fig. 6(c)). Additionally, low signal-to-noise level i.e. low number of electrons contributing to the Ne(2p) signal (Fig. 6(a)) introduces some uncertainty to the form of the spectral amplitude. To estimate an average pulse duration and to eliminate the effect of the noise we have performed the simplified CT pulse retrieval on spectra that were

averaged over all shots (correspondingly all spectra streaked with $+\alpha$, $-\alpha$ and non-streaked VLS spectra were averaged). The retrieved average pulse duration of 82 fs FWHM is substantially shorter than expected from the parameters of the machine operation. Both findings, i.e. a very broad distribution of retrieved pulse durations as well as an underestimated average pulse length, are in correspondence with the results of our numerical study (Fig. 3(b)). Both, numerical study and analysis of experimental results confirm the difficulty to apply the simplified CT for analysis of pulses with complex temporal and spectral pulse profile.

6. Summary

We have applied the Gaussian approximation, the linear streaking as well as the simplified CT approaches in order to retrieve pulse durations of XUV pulses with complex spectral and temporal structures. The single-shot performance of all three pulse retrieval algorithms is compared using numerically generated as well as experimental data. We found no significant difference between the Gaussian approximation and the linear streaking approaches when applied at large streaking speeds. At smaller streaking speeds the Gaussian approach provides a better estimation of the average pulse durations. However, the accuracy for shot-to-shot pulse analysis is decreasing both for the Gaussian and for the linear streaking approaches with decreasing streaking speed as judged by the correlation coefficient. Therefore, we suggest that at large streaking speeds (>25 meV/fs in our case) a reliable estimation of the FEL pulse duration can be reached with linear streaking $\tau_{XUV} = \sigma_{streak}/|\alpha|$ that requires a measurement of only one streaked spectrum and the knowledge of the streaking speed. Considering the linear streaking approach from the user perspective, very fast analysis of τ_{XUV} from the measured spectrum ensures the implementation of this algorithm for efficient XUV pulse diagnostics. Care has to be taken when judging single-shot results. We have found that even at large streaking speed the width of retrieved pulse distributions is substantially broader with respect to the original distribution. In these analyses we have selected numerically generated pulses with a FWHM duration of $100 \text{ fs} \pm 2.5 \text{ fs}$ (standard deviation), the retrieved pulses had a FWHM duration of $100 \text{ fs} \pm 15 \text{ fs}$ (standard deviation). We explain this finding mainly by limitations in defining spectral and temporal widths by the rms values for pulses with a complex structure.

In contrast to the Gaussian and the linear streaking, the implementation of the simplified CT to pulses with complex spectral and temporal structures is difficult. According to the approximation made in Eq. (8) the method is limited to very low streaking speeds. In the case considered here the streaking speed has to be below 5 meV/fs. However, the data analyses at these streaking speeds are very challenging due to a very low electron kinetic energy shift ΔW_{max} as well as due to very small changes of the spectral bandwidth in the streaked spectra (Table 1 and Fig. 6(a)). Moreover, the method is very sensitive to noise in the single-shot spectra because the information on the spectral phase is encoded in the small amplitude changes. In particular, we have found that the noise on the edges of the main photo-line has substantial influence on results of the reconstruction. From the user perspective, this limitation makes the analysis of individual pulses very time consuming. Additionally, the requirement to perform the measurement exactly at the zero-crossing point of the vector potential contributes to the high rejection rate due to the jitter between XUV and THz pulses.

So far the simplified CT algorithm has been implemented in the optical regime for pulses with almost flat spectral phase [43]. The authors found a very good correspondence between the second-order intensity autocorrelation functions retrieved and measured in a non-linear optical crystal. The reconstructed pulse profile is not shown in this study [43]. In the numerical example shown in Ref. [40] the original spectral phase of the pulse contains a combination of a quadratic and third-order terms, however, in the retrieved spectral phase a quadratic term seems to be dominating. Our simulations show that with increasing streaking speed the retrieved pulse length becomes almost independent of the original pulse length. For the numerically generated pulses

the larger pulse duration corresponds to the increasing complexity of the spectral phase due to the limited spectral bandwidth that was kept at the average FWHM of (1.1 ± 0.2) eV (standard deviation). Summarizing these results we suggest that the CT algorithm might be more sensitive to the lower order phase terms and is getting less applicable for pulses with increasing complexity of the spectral phase. Further investigations of the applicability of the simplified CT algorithm for the XUV pulse diagnostics are needed.

In conclusion, we have exploited the THz streak camera performance for single-shot characterization of XUV pulses with complex temporal structure. Results of our numerical study are in correspondence with the analysis of experimental data. We expect that our results will stimulate further development of efficient pulse retrieval algorithms for the single-shot XUV pulse diagnostics techniques at existing and emerging user-facilities based on free-electron lasers or on the generation of high harmonics.

Funding

European Regional Development Fund (CZ.02.1.01/0.0/0.0/15_003/0000447, CZ.02.1.01/0.0/0.0/16_019/0000789); Deutsche Forschungsgemeinschaft (EXC 1074 project ID 194651731).

Acknowledgments

We acknowledge Janos Hajdu for fruitful discussions and continuous interest in the project. The authors would like to thank the scientific and technical team of FLASH for their outstanding support.

This work was supported by the project "Structural dynamics of biomolecular systems (ELIBIO)" (NO. CZ.02.1.01/0.0/0.0/15_003/0000447) from the European Regional Development Fund.

This work was supported by the project "Advanced research using high intensity laser produced photons and particles (ADONIS)" (NO. CZ.02.1.01/0.0/0.0/16_019/0000789) from the European Regional Development Fund.

This work has been supported by "The Hamburg Center for Ultrafast Imaging" of the Deutsche Forschungsgemeinschaft (EXC 1074 project ID 194651731).

Disclosures

The authors declare no conflicts of interest.

References

1. L. Young, K. Ueda, M. Gühr, P. H. Bucksbaum, M. Simon, S. Mukamel, N. Rohringer, K. C. Prince, C. Masciovecchio, M. Meyer, A. Rudenko, D. Rolles, C. Bostedt, M. Fuchs, D. A. Reis, R. Santra, H. Kapteyn, M. Murnane, H. Ibrahim, F. Legare, M. Vrakking, M. Isinger, D. Kroon, M. Gisselbrecht, L. A. Huillier, H. J. Worner, and S. R. Leone, "Roadmap of ultrafast X-ray atomic and molecular physics," *J. Phys. B* **51**(3), 032003 (2018).
2. E. A. Seddon, J. A. Clarke, D. J. Dunning, C. Masciovecchio, C. J. Milne, F. Parmigiani, D. Rugg, J. C. H. Spence, N. R. Thompson, K. Ueda, S. M. Vinko, J. S. Wark, and W. Wurth, "Short-wavelength free-electron laser sources and science: A review," *Rep. Prog. Phys.* **80**(11), 115901 (2017).
3. J. Feldhaus, M. Krikunova, M. Meyer, T. Möller, R. Moshhammer, A. Rudenko, T. Tschentscher, and J. Ullrich, "AMO science at the FLASH and European XFEL free-electron laser facilities," *J. Phys. B* **46**(16), 164002 (2013).
4. R. J. D. Miller, "Femtosecond crystallography with ultrabright electrons and X-rays: Capturing chemistry in action," *Science* **343**(6175), 1108–1116 (2014).
5. B. W. J. McNeil and N. R. Thompson, "X-ray free-electron lasers," *Nat. Photonics* **4**(12), 814–821 (2010).
6. R. Neutze, R. Wouts, D. van der Spoel, E. Weckert, and J. Hajdu, "Potential for biomolecular imaging with femtosecond X-ray pulses," *Nature* **406**(6797), 752–757 (2000).
7. H. N. Chapman, C. Caleman, and N. Timneanu, "Diffraction before destruction," *Phil. Trans. R. Soc. B* **369**(1647), 20130313 (2014).
8. P. J. Ho, B. J. Daurer, M. F. Hantke, J. Bielecki, A. A. Haddad, M. Bucher, G. Doumy, K. R. Ferguson, L. Flückiger, T. Gorkhover, B. Iwan, C. Knight, S. Moeller, T. Osipov, D. Ray, S. H. Southworth, M. Svenda, N. Timneanu, A.

- Ulmer, P. Walter, J. Hajdu, L. Young, F. R. N. C. Maia, and C. Bostedt, "The role of transient resonances for ultra-fast imaging of single sucrose nanoclusters," *Nat. Commun.* **11**(1), 167 (2020).
9. A. A. Sorokin, S. V. Bobashev, T. Feigl, K. Tiedtke, H. Wabnitz, and M. Richter, "Photoelectric effect at ultrahigh intensities," *Phys. Rev. Lett.* **99**(21), 213002 (2007).
 10. L. Young, E. P. Kanter, B. Krässig, Y. Li, A. M. March, S. T. Pratt, R. Santra, S. H. Southworth, N. Rohringer, L. F. DiMauro, G. Doumy, C. A. Roedig, N. Berrah, L. Fang, M. Hoener, P. H. Bucksbaum, J. P. Cryan, S. Ghimire, J. M. Glowia, D. A. Reis, J. D. Bozek, C. Bostedt, and M. Messerschmidt, "Femtosecond electronic response of atoms to ultra-intense X-rays," *Nature* **466**(7302), 56–61 (2010).
 11. M. Krikunova, T. Maltezopoulos, A. Azima, M. Schlie, U. Frühling, H. Redlin, R. Kalms, S. Cunovic, N. M. Kabachnik, M. Wieland, and M. Drescher, "Time-resolved ion spectrometry on xenon with the jitter-compensated soft X-ray pulses of a free-electron laser," *New J. Phys.* **11**(12), 123019 (2009).
 12. T. Oelze, B. Schütte, J. P. Müller, M. Müller, M. Wieland, U. Frühling, M. Drescher, A. Al-Shemmary, T. Golz, N. Stojanovic, and M. Krikunova, "Mapping ultrafast ionization of atoms and clusters with terahertz-streaking delay," *Phys. Rev. A* **99**(4), 043423 (2019).
 13. D. Rupp, L. Flückiger, M. Adolph, T. Gorkhover, M. Krikunova, J. P. Müller, M. Müller, T. Oelze, Y. Ovcharenko, B. Röben, M. Sauppe, S. Schorb, D. Wolter, R. Mitzner, M. Wöstmann, S. Roling, M. Harmand, R. Treusch, M. Arbeiter, T. Fennel, C. Bostedt, and T. Möller, "Recombination-enhanced surface expansion of clusters in intense soft X-ray laser pulses," *Phys. Rev. Lett.* **117**(15), 153401 (2016).
 14. Y. Ovcharenko, V. Lyamayev, R. Katzy, M. Devetta, A. LaForge, P. O'Keeffe, O. Plekan, P. Finetti, M. Di Fraia, M. Mudrich, M. Krikunova, P. Piseri, M. Coreno, N. B. Brauer, T. Mazza, S. Stranges, C. Grazioli, R. Richter, K. C. Prince, M. Drabbels, C. Callegari, F. Stienkemeier, and T. Möller, "Novel collective autoionization process observed in electron spectra of He clusters," *Phys. Rev. Lett.* **112**(7), 073401 (2014).
 15. B. Nagler, U. Zastra, R. R. Fäustlin, S. M. Vinko, T. Whitther, R. S. A. J. Nelson, J. Krzywinski, J. Chalupsky, E. Abreu, S. Bajt, T. Bornath, T. Burian, H. Chapman, J. Cihelka, T. Döppner, S. Düsterer, T. Dzelzainis, M. Fajardo, E. Förster, C. Fortmann, E. Galtier, S. H. Glenzer, S. Göde, G. Gregori, V. Hajkova, P. Heimann, L. Juha, M. Jurek, F. Y. Khattak, A. R. Khorsand, D. Klinger, M. Kozlova, T. Laarmann, H. J. Lee, R. W. Lee, K. H. Meiwes-Broer, P. Mercere, W. J. Murphy, A. Przystawik, R. Redmer, H. Reinholz, D. Riley, G. Röpke, F. Rosmej, K. Saks, R. Schott, R. Thiele, J. Tiggesbäumker, S. Toilekis, T. Tschentscher, I. Uschmann, H. J. Vollmer, and J. S. Wark, "Turning solid aluminium transparent by intense soft X-ray photoionization," *Nat. Phys.* **5**(9), 693–696 (2009).
 16. S. Krinsky and R. L. Gluckstern, "Analysis of statistical correlations and intensity spiking in the self-amplified spontaneous-emission free-electron laser," *Phys. Rev. Spec. Top.—Accel. Beams* **6**(5), 050701 (2003).
 17. C. Behrens, N. Gerasimova, C. Gerth, B. Schmidt, E. A. Schneidmiller, S. Serkez, S. Wesch, and M. V. Yurkov, "Constraints on photon pulse duration from longitudinal electron beam diagnostics at a soft X-ray free-electron laser," *Phys. Rev. Spec. Top.—Accel. Beams* **15**(6), 069902 (2012).
 18. S. Düsterer, M. Rehders, A. Al-Shemmary, C. Behrens, G. Brenner, O. Brovko, M. Dell'Angela, M. Drescher, B. Faatz, J. Feldhaus, U. Frühling, N. Gerasimova, N. Gerken, C. Gerth, T. Golz, A. Grebentsov, E. Hass, K. Honkavaara, V. Kocharian, M. Kurka, T. Limberg, R. Mitzner, R. Moshhammer, E. Plönjes, M. Richter, J. Rönisch-Schulenburg, A. Rudenko, H. Schlarb, B. Schmidt, A. Senftleben, E. Schneidmiller, B. Siemer, F. Sorgenfrei, A. Sorokin, N. Stojanovic, K. Tiedtke, R. Treusch, M. Vogt, M. Wieland, W. Wurth, S. Wesch, M. Yan, M. Yurkov, H. Zacharias, and S. Schreiber, "Development of experimental techniques for the characterization of ultrashort photon pulses of extreme ultraviolet free-electron lasers," *Phys. Rev. Spec. Top.—Accel. Beams* **17**(12), 120702 (2014).
 19. M. Drescher, U. Frühling, M. Krikunova, T. Maltezopoulos, and M. Wieland, "Time-diagnostics for improved dynamics experiments at XUV FELs," *J. Phys. B* **43**(19), 194010 (2010).
 20. W. Helml, I. Grguras, P. N. Juranic, S. Düsterer, T. Mazza, A. R. Maier, N. Hartmann, M. Ilchen, G. Hartmann, L. Patthey, C. Callegari, J. T. Costello, M. Meyer, R. N. Coffee, A. L. Cavalieri, and R. Kienberger, "Ultrashort free-electron laser X-ray pulses," *Appl. Sci.* **7**(9), 915 (2017).
 21. C. Behrens, F. J. Decker, Y. Ding, V. A. Dolgashev, J. Frisch, Z. Huang, P. Krejcik, H. Loos, A. Lutman, T. J. Maxwell, J. Turner, J. Wang, M. H. Wang, J. Welch, and J. Wu, "Few-femtosecond time-resolved measurements of X-ray free-electron lasers," *Nat. Commun.* **5**(1), 3762 (2014).
 22. A. Sanchez-Gonzalez, P. Micaelli, C. Olivier, T. R. Barillot, M. Ilchen, A. A. Lutman, A. Marinelli, T. Maxwell, A. Achner, M. Agåker, N. Berrah, C. Bostedt, J. D. Bozek, J. Buck, P. H. Bucksbaum, S. C. Montero, B. Cooper, J. P. Cryan, M. Dong, R. Feifel, L. J. Frasinski, H. Fukuzawa, A. Galler, G. Hartmann, N. Hartmann, W. Helml, A. S. Johnson, A. Knie, A. O. Lindahl, J. Liu, K. Motomura, M. Mücke, C. OGrady, J.-E. Rubensson, E. R. Simpson, R. J. Squibb, C. Sätke, K. Ueda, M. Vacher, D. J. Walke, V. Zhaunerchyk, R. N. Coffee, and J. P. Marangos, "Accurate prediction of X-ray pulse properties from a free-electron laser using machine learning," *Nat. Commun.* **8**(1), 15461 (2017).
 23. C. Gahl, A. Azima, M. Beye, M. Deppe, K. Döbrich, U. Hasslinger, F. Hennies, A. Melnikov, M. Nagasono, A. Pietzsch, M. Wolf, W. Wurth, and A. Föhlisch, "A femtosecond X-ray/optical cross-correlator," *Nat. Photonics* **2**(3), 165–169 (2008).
 24. T. Maltezopoulos, S. Cunovic, M. Wieland, M. Beye, A. Azima, H. Redlin, M. Krikunova, R. Kalms, U. Frühling, F. Budzyn, W. Wurth, A. Föhlisch, and M. Drescher, "Single-shot timing measurement of extreme-ultraviolet free-electron laser pulses," *New J. Phys.* **10**(3), 033026 (2008).

25. R. Riedel, A. Al-Shemmary, M. Gensch, T. Golz, M. Harmand, N. Medvedev, M. J. Prandolini, K. Sokolowski-Tinten, S. Toleikis, U. Wegner, B. Ziaja, N. Stojanovic, and F. Tavella, "Single-shot pulse duration monitor for extreme ultraviolet and X-ray free-electron lasers," *Nat. Commun.* **4**(1), 1731 (2013).
26. P. Radcliffe, S. Düsterer, A. Azima, H. Redlin, J. Feldhaus, J. Dardis, K. Kavanagh, H. Luna, J. P. Gutierrez, P. Yeates, E. T. Kennedy, J. T. Costello, A. Delsierys, C. L. S. Lewis, R. Taïeb, A. Maquet, D. Cubaynes, and M. Meyer, "Single-shot characterization of independent femtosecond extreme ultraviolet free electron and infrared laser pulses," *Appl. Phys. Lett.* **90**(13), 131108 (2007).
27. S. Cunovic, N. Müller, R. Kalms, M. Krikunova, M. Wieland, M. Drescher, T. Maltezopoulos, U. Fröhling, H. Redlin, E. Plönjes-Palm, and J. Feldhaus, "Time-to-space mapping in a gas medium for the temporal characterization of vacuum-ultraviolet pulses," *Appl. Phys. Lett.* **90**(12), 121112 (2007).
28. M. Drescher, M. Hentschel, R. Kienberger, M. Uiberacker, V. Yakovlev, A. Scrinzi, T. Westerwalbesloh, U. Kleineberg, U. Heinzmann, and F. Krausz, "Time-resolved atomic inner-shell spectroscopy," *Nature* **419**(6909), 803–807 (2002).
29. F. Krausz and M. Ivanov, "Attosecond physics," *Rev. Mod. Phys.* **81**(1), 163–234 (2009).
30. U. Fröhling, M. Wieland, M. Gensch, T. Gebert, B. Schütte, M. Krikunova, R. Kalms, F. Budzyn, O. Grimm, J. Rossbach, E. Ploenjes, and M. Drescher, "Single-shot terahertz-field-driven X-ray streak camera," *Nat. Photonics* **3**(9), 523–528 (2009).
31. I. Grguras, A. R. Maier, C. Behrens, T. Mazza, T. J. Kelly, P. Radcliffe, S. Düsterer, A. K. Kazansky, N. M. Kabachnik, T. Tschentscher, J. T. Costello, M. Meyer, M. C. Hoffmann, H. Schlarb, and A. L. Cavalieri, "Ultrafast X-ray pulse characterization at free-electron lasers," *Nat. Photonics* **6**(12), 852–857 (2012).
32. B. Schütte, U. Fröhling, M. Wieland, A. Azima, and M. Drescher, "Electron wave packet sampling with laser-generated extreme ultraviolet and terahertz fields," *Opt. Express* **19**(20), 18833 (2011).
33. F. Ardana-Lamas, C. Erny, A. G. Stepanov, I. Gorgisyan, P. J. and R. Abela, and C. P. Hauri, "Temporal characterization of individual harmonics of an attosecond pulse train by THz streaking," *Phys. Rev. A* **93**(4), 043838 (2016).
34. P. N. Juranic, A. Stepanov, R. Ischebeck, V. Schlott, C. Pradervand, L. Patthey, M. Radovic, I. Gorgisyan, L. Rivkin, C. P. Hauri, B. Monoszalai, R. Ivanov, P. Peier, J. Liu, T. Togashi, S. Owada, K. Ogawa, T. Katayama, M. Yabashi, and R. Abela, "High-precision x-ray FEL pulse arrival time measurements at SACLA by a THz streak camera with Xe clusters," *Opt. Express* **22**(24), 30004–30012 (2014).
35. I. Gorgisyan, R. Ischebeck, C. Erny, A. Dax, L. Patthey, C. Pradervand, L. Sala, C. Milne, H. T. Lemke, C. P. Hauri, T. Katayama, S. Owada, M. Yabashi, T. Togashi, R. Abela, L. Rivkin, and P. Juranic, "THz streak camera method for synchronous arrival time measurement of two-color hard X-ray FEL pulses," *Opt. Express* **25**(3), 2080–2091 (2017).
36. R. Ivanov, J. Liu, G. Brenner, M. Brachmanskia, and S. Düsterer, "FLASH free-electron laser single-shot temporal diagnostic: terahertz-field-driven streaking," *J. Synchrotron Radiat.* **25**(1), 26–31 (2018).
37. U. Fröhling, "Light-field streaking for FELs," *J. Phys. B* **44**(24), 243001 (2011).
38. A. Azima, J. Bödewadt, O. Becker, S. Düsterer, N. Ekanayake, R. Ivanov, M. M. Kazemi, L. L. Lazzarino, C. Lechner, T. Maltezopoulos, B. Manschwetus, V. Milchev, J. Müller, T. Plath, A. Przystawik, M. Wieland, R. Assmann, I. Hartl, T. Laarmann, J. Rossbach, W. Wurth, and M. Drescher, "Direct measurement of the pulse duration and frequency chirp of seeded XUV free electron laser pulses," *New J. Phys.* **20**(1), 013010 (2018).
39. J. Itatani, F. Quere, G. L. Yudin, M. Y. Ivanov, F. Krausz, and P. B. Corkum, "Attosecond streak camera," *Phys. Rev. Lett.* **88**(17), 173903 (2002).
40. F. Quere, Y. Mairesse, and J. Itatani, "Temporal characterization of attosecond XUV fields," *J. Mod. Opt.* **52**(2–3), 339–360 (2005).
41. Y. Mairesse and F. Quere, "Frequency-resolved optical gating for complete reconstruction of attosecond bursts," *Phys. Rev. A* **71**(1), 011401 (2005).
42. W. Helml, A. R. Maier, W. Schweinberger, I. Grguras, P. Radcliffe, G. Doumy, C. Roedig, J. Gagnon, M. Messerschmidt, S. Schorb, C. Bostedt, F. Grüner, L. F. DiMauro, D. Cubaynes, J. D. Bozek, T. Tschentscher, J. T. Costello, M. Meyer, R. Coffee, S. Düsterer, A. L. Cavalieri, and R. Kienberger, "Measuring the temporal structure of few-femtosecond free-electron laser X-ray pulses directly in the time domain," *Nat. Photonics* **8**(12), 950–957 (2014).
43. C. Dorrer and I. Kang, "Complete temporal characterization of short optical pulses by simplified chronocyclic tomography," *Opt. Lett.* **28**(16), 1481–1483 (2003).
44. I. A. Walmsley and C. Dorrer, "Characterization of ultrashort electromagnetic pulses," *Adv. Opt. Photonics* **1**(2), 308–437 (2009).
45. J. Feldhaus, J. Arthur, and J. B. Hastings, "X-ray free-electron lasers," *Adv. Opt. Photonics* **38**(9), S799–S819 (2005).
46. T. Pfeifer, Y. Jiang, S. Düsterer, R. Moshhammer, and J. Ullrich, "Partial-coherence method to model experimental free-electron laser pulse statistics," *Opt. Lett.* **35**(20), 3441–3443 (2010).
47. K. Tiedtke, A. Azima, N. von Bargaen, L. Bittner, S. Bonfigt, S. Düsterer, B. Faatz, U. Fröhling, M. Gensch, C. Gerth, N. Guerassimova, U. Hahn, T. Hans, M. Hesse, K. Honkavaar, U. Jastrow, P. Juranic, S. Kapitzki, B. Keitel, T. Kracht, M. Kuhlmann, W. B. Li, M. Martins, T. Núez, E. Plönjes, H. Redlin, E. L. Saldin, E. A. Schneidmiller, J. R. Schneider, S. Schreiber, N. Stojanovic, F. Tavella, S. Toleikis, R. Treusch, H. Weigelt, M. Wellhöfer, H. Wabnitz, M. V. Yurkov, and J. Feldhaus, "The soft x-ray free-electron laser FLASH at DESY: beamlines, diagnostics and end-stations," *New J. Phys.* **11**(2), 023029 (2009).
48. R. Pan, E. Zapolnova, T. Golz, A. J. Krmpot, M. D. Rabasovic, J. Petrovic, V. Asgekar, B. Faatz, F. Tavella, A. Perucchi, S. Kovalev, B. Green, G. Geloni, T. Tanikawa, M. Yurkov, E. Schneidmiller, M. Gensch, and N. Stojanovic, "Photon diagnostics at the FLASH THz beamline," *J. Synchrotron Radiat.* **26**(3), 700–707 (2019).

49. G. Brenner, S. Kapitzki, M. Kuhlmann, E. Ploenjes, T. Noll, F. Siewert, R. Treusch, K. Tiedtke, R. Reininger, M. Roper, M. Bowler, F. Quinn, and J. Feldhaus, "First results from the online variable line spacing grating spectrometer at flash," *Nucl. Instrum. Methods Phys. Res., Sect. A* **635**(1), S99–S103 (2011).